Nanoscale

Accepted Manuscript

This article can be cited before page numbers have been issued, to do this please use: E. Gonzalez-Lavado , N. Iturrioz-Rodriguez, E. Padin-González, J. A. Gonzalez, L. Garcia-Hervia, J. Heuts, C. Pesquera, F. Gonzalez, J. C. Villegas, R. Valiente and M. L. Fanarraga, *Nanoscale*, 2018, DOI: 10.1039/C8NR03036G.

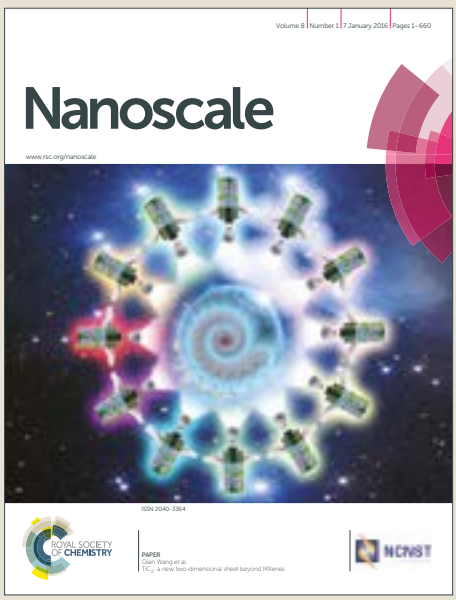

ROYAL SOCIETY OF CHEMISTRY

rsc.li/nanoscale

Biodegradable multi-walled carbon nanotubes trigger anti-tumoral effects

View Article Online
DOI: 10.1039/C8NR03036G

E. González-Lavado,[a] N. Iturrioz-Rodríguez,[a] E. Padín-González,[a] J. González,[a] L. García-Hevia,[b] J. Heuts,[a] C. Pesquera,[a] F. González,[a] J. C. Villegas,[a] R. Valiente,[a] M. L. Fanarraga[a]

Received 00th January 20xx,
Accepted 00th January 20xx

DOI: 10.1039/x0xx00000x

www.rsc.org/

Carbon nanotubes have a huge biotechnological interest because they can penetrate most biological barriers and, inside cells, can biomimetically interact with the cytoskeletal filaments, triggering anti-proliferative and cytotoxic effects in highly dividing cells. Unfortunately, their intrinsic properties and bio-persistence represent a putative hazard that relapses their application as therapies against cancer. Here we investigate mild oxidation treatments to improve MWCNTs intracellular enzymatic digestion, but preserving their morphology, responsible for their intrinsic anti-cancer properties. Cell imaging techniques and confocal Raman spectroscopic signature analysis revealed that cultured macrophages can degrade bundles of oxidized MWCNTs (o-MWCNTs) in a few days. Isolation of nanotubes from these phagocytes 96 hours after exposure confirmed a significant reduction of approximately 30% in the total length of these filaments compared to control o-MWCNTs extracted from the cell culture medium, or the intracellular pristine MWCNTs. More interestingly, *in vivo* single intratumoral injections of o-MWCNTs triggered ca. 30% solid melanoma tumour growth-inhibitory effects while displaying significant signs of biodegradation at the tumoral/peri-tumoral tissues a week after the therapy has had the effect. These results support the potential use of o-MWCNTs as antitumoral agents and reveal interesting clues of how to enhance *in vivo* carbon nanotube efficient clearance.

Introduction

Carbon nanotubes (CNTs) are likely to participate in many new ground-breaking advances in nanomedicine including drug/gene delivery, tissue regeneration, bio-sensing, probes for diagnostics or monitoring, among many others.[1] CNTs are also interesting tools for therapeutic delivery since they can move across most cellular barriers, interact with tissues in living organisms, finally translocating inside the cells, where they interact with different organelles and proteins.[2–4] These intrinsic properties of CNTs have a great potential if they are exploited in biotechnology.[5–9]

Among CNTs, multiwalled carbon nanotubes (MWCNTs) display unique biomimetic properties with microtubules[10,11] that are well-established targets for many anticancer drugs such as taxol®.[12] Microtubules are highly dynamic intracellular tubulin protein nanotubes that play a central role in cell division and migration. These protein filaments and MWCNTs (i) self-assemble, (ii) have analogous dimensions, (iii) are exceptionally resilient and finally, (iv) show comparable extraordinary structural and surface properties (i.e. shear stress, bending stiffness, Young´s modulus).[10,13,14]

Similarities between MWCNTs and microtubules prompt their interaction *in vitro*[15] and *in vivo*[11,16] and the assembly of mixed bio-synthetic intracellular polymers that display an enhanced stability compared to conventional tubulin polymers.[11] This interaction triggers critical changes in the cellular biomechanics resulting in anti-proliferative,[11] anti-migratory[17,18] and cytotoxic[19] effects in cancer cells *in vitro*, as well as significant anti-tumoral effects *in vivo*.[20] These results suggest CNTs could have a potential application as adjuvant or neoadjuvant therapies in the development of future anti-cancer agents.[21] Unfortunately, despite these interesting results, there is a long way before MWCNTs can be applied to humans. Their potential long-term effects due to tissue damage and accumulation are key issues to control and improve. Among the unwanted side effects in healthy cells and tissues, MWCNTs trigger: inflammatory reactions, cytotoxicity, DNA breakage, chromosomal mal-segregation, etc.[22–26] Thus, the “Achilles heels” for the potential applications of MWCNTs as nanomedicines is the complete inactivation and/or clearance of these nanomaterials after therapy.

The discovery of CNT bio-degradation *in vitro* by phagocytic cells has opened new opportunities. These cells have an extraordinary degradative potential, and can break down virtually all kinds of biomolecules captured by the endocytic or phagocytic entry routes. Their lysosomes, apart from displaying a pH of 4.5, contain a large variety of enzymes (acid-hydrolases and peroxidases) that are able to gradually digest CNTs.[27–33] Macrophages,[32] microglia,[33–36] neutrophils[37,38] and eosinophils[31] have all been confirmed to degrade CNTs in culture after different previous surface treatments. Paradoxically, phagocytes are more susceptible than other cells to CNT-toxicity, at least *in vitro*.[19,39] Their avidity to capture these foreign materials often results in the production of intolerable levels of superoxides and hydroxyl radicals involved in the oxidative stress reaction triggered during CNT degradation.[25,32,35,40–42]

Some studies support the idea that reaching an equilibrium between phagocyte nanotube intake and clearance is critical to prevent tissue bioaccumulation and damage. But improving MWCNT biodegradation is not a trivial task. These fibres are

[a] Grupo de Nanomedicina Universidad de Cantabria-IDIVAL, Herrera Oria s/n, 39011, Santander, Spain.
[b] INL, Avda. Maestre José Veiga, 4715-403 Braga, Portugal.
[c] Electronic Supplementary Information (ESI) available: [details of any supplementary information available should be included here]. See DOI: 10.1039/x0xx00000x

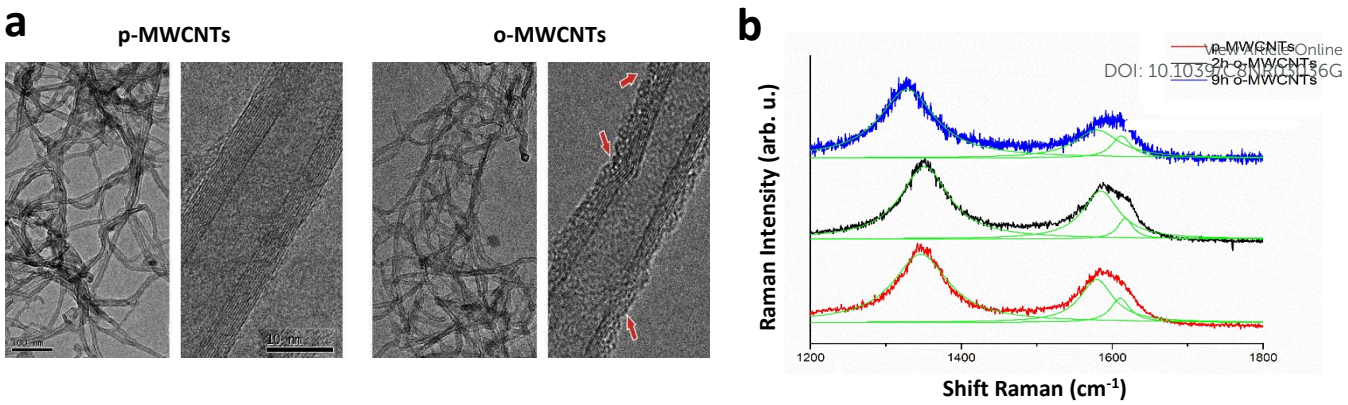

Fig. 1. Characterization of the o-MWCNTs. **(a)** Low and high-resolution transmission electron microscopy (TEM) pictures of p-MWCNTs and 9 h o-MWCNTs demonstrating a general preservation of the morphology but small defects on the outer o-MWCNT walls (arrows). **(b)** Raman spectra of p-MWCNTs and o-MWCNTs (2 h and 9 h) samples. The Lorentzian curves (green) fitting used for peak area determination are also shown.

some of the strongest and stiffest materials and thus, they are highly stable under standard *in vivo* physiological conditions. Their bio-persistence depends on (i) the number of walls of the nanotube, (ii) the surface and diameter of the tubes, (iii) the dose, (iv) route of administration and finally, (v) their surface functionalisation.[24,26,43–46] Interestingly, several studies show how CNT degradation by biological enzymes is significantly enhanced when the nanotube surface is chemically modified by oxidation.[34,35,45,47–51] This treatment results in the formation of different functional groups on the CNT surface, and structural defects in the nanotube walls that serve as macrophage enzymatic "attack" sites for wall degradation.

Based on these findings, we have explored various surface oxidation pre-treatments to enhance MWCNT clearance by macrophages preserving their biomimetic properties with microtubules, in ultimate term responsible for their anti-proliferative, anti-migratory and cytotoxic effects in cancer cells.

Results and discussion

MWCNT oxidation pre-treatment.

To improve intracellular CNT degradation, pristine MWCNTs (p-MWCNTs) were oxidized in a v/v = 3/1 mixture of H_2SO_4/HNO_3 at 37º C for two different periods of time (2 and 9 h, as indicated). As described elsewhere,[52] this treatment generates the formation of functional groups such as –C–OH groups that can be transformed into –C=O groups on the outer surface of the oxidized MWCNTs (o-MWCNTs). To characterize this process and to obtain valuable information about the structure, composition and surface adsorbed molecules and defects on o-MWCNTs we employed transmission electron microscopy (TEM) and Raman spectroscopy to characterize the degree of structural defects/changes and to monitor the different vibrational active modes produced by the oxidation processes (see also **Fig. S1**).[53,54]

TEM imaging of the p-MWCNTs and the 9h o-MWCNTs (**Fig. 1a**) revealed defects including: (i) a reduction of the number of walls, from 12-16 walls in pristine sample to 8-10 average carbon layers in o-MWCNTs, (ii) changes in the outer and inner walls, (iii) layer exfoliation, (iv) small surface imperfections and finally, (v) wall bending or breaks. This technique also served to demonstrate a general good preservation of the o-MWCNTs (i.e. diameter and length, see below).

Raman spectroscopy, yields key information of the purity and defects of the MWCNTs, allowing the identification of this type of nanotubes among other carbon compounds. In particular, the measurement of the integrated intensity ratio between the D and G bands (A_D/A_G) is a way to semi-quantify the degree of structural defects in the nanotube sample (Table 1).[33,34,36,45,55,56] **Fig. 1b** displays representative Raman spectra of p-MWCNT, 2 and 9 h pre-oxidized MWCNT samples showing the characteristic D and G bands at ca. 1350 cm^{-1} and 1590 cm^{-1}, respectively. These bands represent a good fingerprint of the graphitization of the sample, where the D band is assigned to the presence of disorder, and the G band corresponds to the tangential vibrations of carbon atoms along the layer. The D´ band, at ca. 1615 cm^{-1} can also be observed as a shoulder attached to the G band. Interestingly, the G band shifts towards lower wavenumbers with longer oxidation treatments indicating the charge transfer produced by the processes of oxidation and degradation modifying the charge at the MWCNT surface.[57,58] Based on these studies, we compared the A_D/A_G integrated intensity ratios of p-MWCNTs, 2 h and 9 h o-MWCNTs to estimate the degree of surface defects triggered by the oxidation pre-treatment on the surface of the nanotubes samples. Results summarized in Table 1 confirmed a relationship between the oxidation time and the structural defects on the surface of the nanotubes, validating the effectiveness of the applied treatment.

	p-MWCNT	o-MWCNT	
		2 h	9 h
A_D/A_G	-		
	2.29	2.32	2.79

Table 1. Analysis of the A_D/A_G ratios for pristine (p-MWCNTs), 2 h and 9 h oxidized (o-MWCNTs) nanotubes

Improved o-MWCNTs degradation by cultured macrophages.

MWCNTs used as anti-tumoral agents should normally be degraded at the tumour site by the tumour-associated-macrophages and/or local stromal cells. Thus, to evaluate the improved biodegradation of MWCNTs bundles inside these cells, we used phase contrast microscopy on immortalized macrophages exposed to 5 µg/mL of 2 h and 9 h o-MWCNTs in the culture medium. As **Fig. S2** shows, macrophages exposed during 72 h to 9 h o-MWCNTs displayed a significant reduction of the intracellular black-carbon masses compared to identical cells exposed to 2 h o-MWCNTs. As observed by other authors,[59] MWCNT oxidation was also accompanied by an improved phagocyte survival rate (**Fig. S2c**).

The intracellular degradation process was verified using other techniques. To further confirm intracellular o-MWCNT degradation, we extracted nanotubes from the cells exposed to 9 h o-MWCNTs or p-MWCNTs during 96 h (see the Experimental section). Extracted nanotubes were compared to the *as prepared* original nanotubes characterised in Fig. 1, and the nanotubes present in the culture medium where macrophages were growing (see the experimental diagram in **Fig. S3**). Nanotubes extracted from cells, the culture media and the *as prepared* material were photographed using TEM (**Fig. 2**) and were measured to evaluate degradation. Quantitative and qualitative analysis of these nanotube samples demonstrated a significant reduction in the total lengths of the intracellular o-MWCNTs indicative of intracellular degradation.

As an additional technique, we use confocal Raman spectroscopy, focusing the laser beam spot within the carbon-containing phagosomes in the cytoplasm of macrophages (white cross in Fig. S2) to investigate degradation. As in the previous study, we semi-quantified degradation calculating the A_D/A_G ratios at different times (12, 24, 48, 72 and 96 h) recording the signatures of the D and G bands in the wavelength range 1200-1800 cm^{-1} (**Figs. 2, S4**) in a total of 10-20 randomly taken intracellular spots of 1 μm^2 area. Results shown in Fig. 2b suggest that 9h o-MWCNTs begin biodegradation in macrophages soon after phagocytosis.

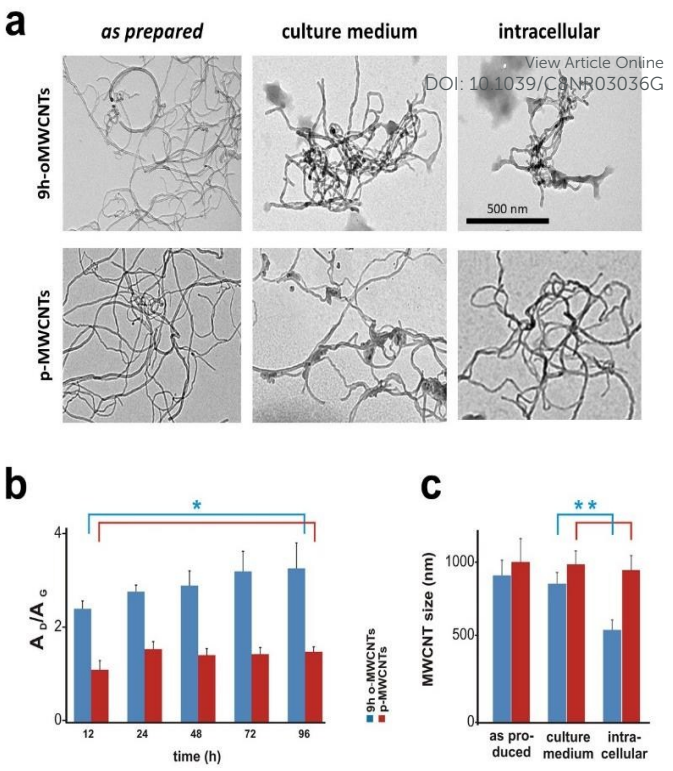

Fig. 2. o-MWCNTs are processed inside macrophages. (a) TEM images of the *as prepared* o-MWCNTs or p-MWCNTs, and identical nanotubes extracted from the culture medium or from macrophages 96 h after incubation (see **Fig. S3**). All images display identical magnification. **(b)** Semi-quantification of the structural defects on intracellular nanotubes using Raman spectroscopy (results from spectrograms in **Fig. S4**) (oMWCNTs t= 1.86; n= 28; pMWCNTs t= 1.84; n= 22; *= $t_{.95}$). **(c)** Quantification of the average lengths of the different nanotube samples. o-MWCNTs isolated from inside macrophages displayed significantly smaller sizes (t= 2.98 n = 59; **= $t_{.995}$) that those obtained from the culture medium of the phagocytes. On the contrary, p-MWCNTs did not shortened inside macrophages after 96 h (t= 0.26 n = 58).

o-MWCNT display biomimetic anticancer cytotoxic effects *in vitro*.

We now tested the anti-cancer cytotoxic effects of o-MWCNTs on HeLa cells following previously published protocols.[11] Confocal microscopy examination of 50 µg/mL o-MWCNT treated cell cultures served to confirm sings indicative of the biomechanical disruptive effect of these nanotubes on HeLa, including: (i) cell retraction, (ii) membrane blebbing, (iii) nuclear DNA compaction, (iv) presence of micronuclei (**Figs. 3a** -white asterisks, **S5**), as well as other previously described cytoskeletal changes including a disorganized microtubular patterns or a reactive cortical actin.[18] Interestingly, many cells presented long extra-cellular actin/tubulin-coated extensions, measuring 10-15 µm, similar to those shown to contain MWCNTs in previous studies (red-green arrows).[11] Similar experiments were also performed in parallel on malignant cancer cells. For this purpose we selected the B16-F10 murine cell line, a multi-resistant malignant melanoma that displays an aggressive nature, is genetically heterogeneous and is highly metastatic (**Fig S6**).[60]

o-MWCNTs inhibit tumour progression *in vivo* in a mouse model and degrade in the tumoral tissues.

The anti-tumoral effects of o-MWCNTs were tested on solid melanoma tumours produced by transplantation of B16-F10 cells. This system model is highly representative of most malignant tumours, being characterized by local acidosis, oedema and abundant tumour-associated supporting stromal cells that include macrophages.[60,61] To improve reproducibility, solid pigmented melanoma tumours were injected only once with 2 µg of serum-functionalised nanotubes resuspended in a saline solution containing antibiotics (see the Experimental section). Intra-tumoral injection experiments were performed systematically in total population of more than 150 transplanted mice (see below) that were sacrificed 4 days post-injection. As a control, we injected the resuspension medium in sibling mice obtained from the same litter. Results shown in **Fig. 3b-c** demonstrate a patent tumoral size reduction in o-MWCNT treated animals compared to controls. Melanoma mass quantification revealed a ca. 30 % weight reduction in o-

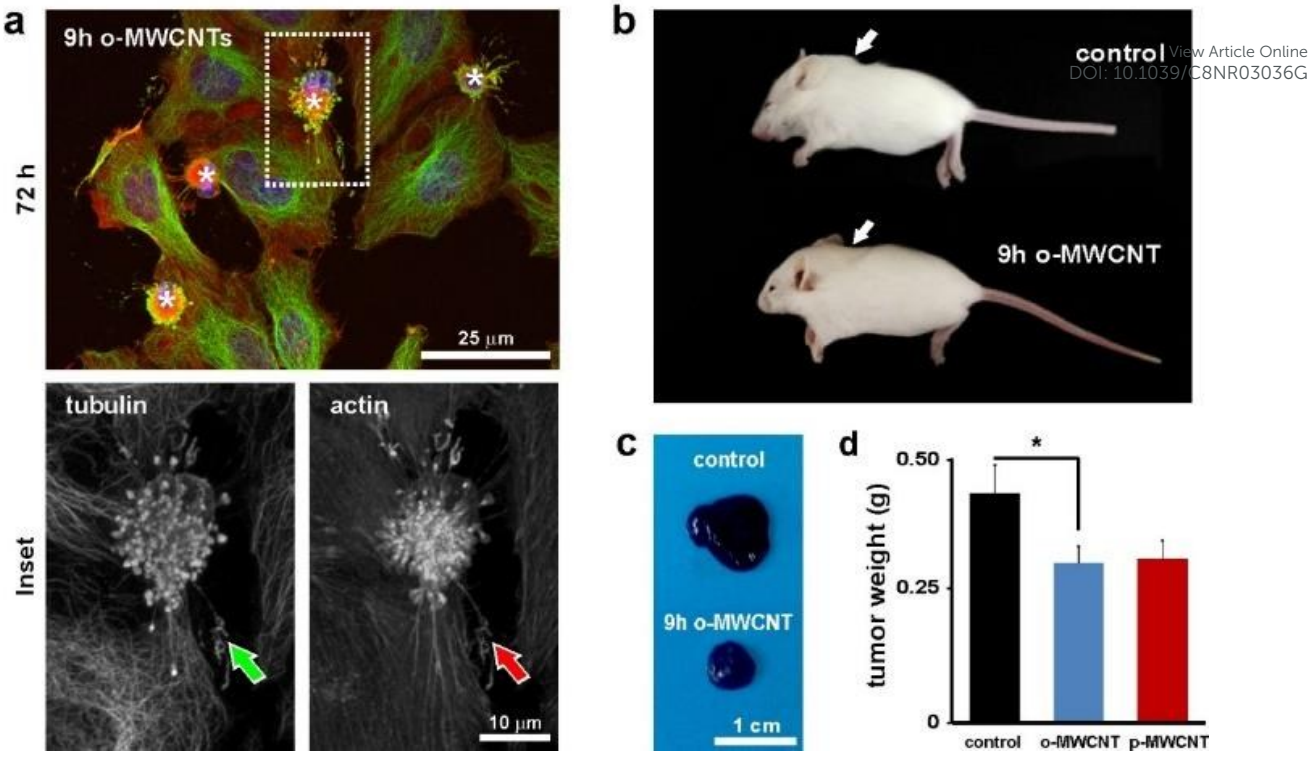

Fig.3. ***In vitro*** **and** ***in vivo*** **o-MWCNTs effects**. **(a)** Confocal microscopy projection images of HeLa cells exposed to o-MWCNTs for 72 h. Representative image demonstrating the apoptotic effect o-MWCNTs. Dying cells (white asterisk) typically display signs indicative of apoptosis. Acentrosomal microtubule networks (green channel) and actin microfilament reorganization (red channel) are also patent in most cells. (inset) Apoptotic cells show abnormally long cytoplasmic extensions labelled for tubulin (green arrow) and actin (red arrow). **(b)** Antineoplastic effect of o-MWCNTs in solid melanoma tumours. Representative mouse littermates bearing solid melanoma tumours 96 h after a single intra-tumoral injection of resuspension medium (control) or o-MWCNTs post treatment. Arrows point at the tumour location. **(c)** Representative solid pigmented melanoma tumoral masses, 96 h after a single injection containing 2 μg o-MWCNT treatment. **(d)** Statistical evaluation of the average tumoral size 96 h post-treatment (single injection containing 2 μg o-MWCNT). Biodegradable o-MWCNTs trigger a statistically significant anti-tumoral effect (t= 1.5 n= 146; *= $t_{.90}$) but indistinguishable to that observed for p-MWCNTs.

MWCNT-treated tumours significant (t= 1.5; n= 146, **Fig. 3d**). This anti-tumoral effect was undistinguishable to that observed in mice injected with p-MWCNTs (t= 0.2; n= 161). Finally, the biodegradability of the injected nanotubes at the tumoral organ was evaluated using Raman spectroscopy. Semi-quantification of the A_D/A_G bands in peritumoral and intratumoral tissue sections revealed a significant degradation of the injected o-MWCNTs *in situ*, 18 and 15 days after injection respectively, while no significant changes were observed for p-MWCNTs as these time points (**Fig. 4**).

Summarizing, here we present a bio-compatibilization method that can be used to improve the risk-to-benefit ratio of MWCNTs for their potential used as nanomedicines against cancer, either as adjuvant or as neoadjuvant therapies. Moreover, identical pre-treatments can be used for nanotubes used as surface coatings in the assembly of multi-structured nanodelivery carrier devices to improve intracellular cytoplasmic targeting.[8]

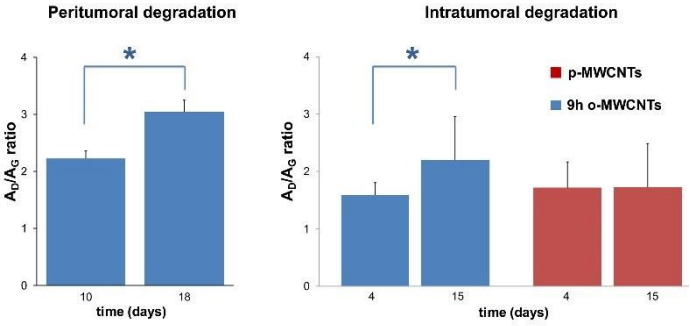

Fig. 4. Raman spectroscopic semi-quantitative analysis of o-MWCNT degradation in the tumoral organ. Time indicates days post injection. Pre-oxidized MWCNTs show a patent peritumoral (t= 1.6 n= 29; *= $t_{.90}$) and intratumoral (t= 1.4; n= 6; *= $t_{.90}$) biodegradation compared to p-MWCNTs (t= 0.01; n= 5).

Experimental

MWCNT oxidation and characterization.

High-purity MWCNT obtained from Nanocyl NC3100™ were dispersed by sonication for 5 minutes in a 3:1 mixture of H_2SO_4 (98%)/HNO_3 (65%) and were incubated at 37º C under continuous shaking.[26,45] Resulting *as prepared* MWCNTs were fully characterised by Raman and IR spectroscopy, TGA, mass spectrometry and TEM (**Fig. S1**). Samples were taken at 2 or 9 h. The acid solution was removed by filtration through a 0.45 µm and were washed in H_2O until pH ~7. o-MWCNTs were dispersed and functionalised with serum-containing culture medium as previously described.[11] Final working solutions were centrifuged 2 min. at 10,000 g to remove micrometric aggregates before concentration determination by optical absorption at 550 nm. Raman spectra were taken with a Horiba T64000 triple spectrometer in the backscattering geometry, a 647 nm line of a Coherent Innova Spectrum 70c Ar^+–Kr^+ laser and a nitrogen-cooled CCD (Jobin-Yvon Symphony). A confocal microscope was used for the intracellular sample Raman spectra detection focusing the laser beam into a 1 μm^2 with a 100x objective as described in previous studies.[11] MWCNT were identified using unique fingerprints characterizing a number of well-defined resonances[55] such as the dispersive disorder induced D band, the tangential G and the D' band, which are attributed using the symmetry analysis to the longitudinal optical mode (LO) close to Brillouin zone centre (Γ).[62] The D-band representing the asymmetrical properties of the tubes (structural defects), and the G-band the planar carbon atom vibrations (linear structure). Raman features such as the radial breaching modes (RBM), associated with a small diameter inner tube (less than 2 nm), are usually too weak to be observable in these large diameter tubes.[63,64] As for previous studies, the ratio between the areas of the intensity the D and G peaks (A_D/A_G) were used to characterize the structural disorganization that MWCNTs undergo during oxidation and intracellular degradation.[32–34,45] The average intensities of more than 10 spectra for each time and MWCNT type and experimental time are represented in histograms of Fig. 2c. Transmission electron microscopy was performed in a JEOL JEM 2100 operated at 120 kV on ethanol-dispersed samples adsorbed onto a Lacey copper grid. Infrared spectra were recorded on a Jasco LE4200 spectrophotometer. TGA was carried out using a Setaram Setsys Evolution 1700 apparatus, ranging from ca 20 - 900º C. Samples were placed into platinum crucibles. Measurements were performed in nitrogen atmosphere with a heating rate of 10 º C/min at a total flow rate of 20 mL/min. A mass spectrometer, Pfeiffer OmniStar Prisma, attached to the TG equipment allowed us to follow the exhausted CO_2 gas.

Cell culture and viability studies.

HeLa and murine macrophage cells (J774) were grown in cultured with Eagle's Minimum Essential Medium (EMEM, Biowhittaker™) and Iscove's Modified Dulbecco's Medium (IMDM) respectively, containing 10% FBS, and were kept in standard conditions. HeLa and J774 cells were exposed to 50 and 5 µg/mL respectively. Live/dead cell assessment was performed automatically using a trypan blue assay (Sigma-Aldrich) on a Bio-Rad TC-20 cell counter at the indicated times. An average of 540,000 macrophage cells were automatically counted for each condition.

MWCNT isolation from cells/medium.

Macrophage cells were exposed to nanotubes in the culture medium for 96 h before extraction. Identical amounts of cells (ca. 9 x 10^6 cells of each) and culture medium (500 µL of medium originally containing 50 µg/mL of nanotubes) were used for nanotube isolation. After cell pelleting, the culture media containing the resuspended MWCNTs and the cell pellets were processed in parallel for direct comparison. Samples were treated successively with 1% Triton X100 phosphate buffered saline (PBS), 35% HCl and acetone.

Statistical analysis.

A two-tailed *t*-test was used in all other statistical analysis. Significance was stablished for a p= 0.05 (*) or a p= 0.01 (**).

Imaging studies.

Cells were fixed with 4% paraformaldehyde. Actin was stained with Phalloidin-Tetramethylrhodamine B isothiocynate and the DNA with Hoechst dye (both from Sigma-Aldrich®). Microtubules were immunostained with B512 anti- α-tubulin antibody (Sigma-Aldrich®) and a secondary goat anti-mouse IgG antibody conjugated with Alexa Fluor 488 (Molecular probes®). Confocal and phase contrast images were taken using a Nikon A1R confocal microscope. Image processing was performed with the NIS-Elements Advanced Research software. Fluorescent images are pseudo-coloured.

o-MWCNT tumour growth studies *in vivo.*

Tumorigenesis was induced by subcutaneous transplantation of a total of 2x10^5 B16-F10 melanoma cells in 10 µL of culture medium containing antibiotics following previously described procedures.[64] Animal experimentation procedures were performed according to EU legislation. All animal procedures were performed in accordance with the Guidelines for Care and Use of Laboratory Animals of The University of Cantabria and approved by the Animal Ethics Committee of this University. Solid pigmented tumours were single treated 7 days post-transplant with a unique dose of 2 µg of o-MWCNTs resuspended in a volume of 10 µL of culture medium. To reduce natural artefacts, littermates were injected in parallel with o-MWCNTs or the resuspension medium used as excipient. Tumours masses were carefully dissected and weighed 4 days post injection. Statistical analysis was performed using a *t*-test. The confidence levels and total number of events included in the study (n) are indicated in the figures. Quantitative results are expressed as mean values with their corresponding standard deviation error bars.

Conclusions

In conclusion, here we demonstrate o-MWCNT biodegradation in cultured cells and *in vivo*, at the tumoral site in mice bearing malignant tumours produced by transplantation. Biodegradation is detectable a few days after these nanotubes have had a therapeutic effect. This new property can serve to synergistically improve the already existing traditional microtubule-stabilizing chemotherapies such as taxol®, but also to enhance the *in vivo* degradation of carbon nanotubes as key components in the design of novel nanocarrier devices for their use in therapeutic fields other than cancer.

Current affiliations

Dr. L. García-Hevia, International Iberian Nanotechnology Institute, Braga, Portugal; Mr. J. Heuts, Leiden University, The Hague, The Netherlands.

Conflicts of interest

There are no conflicts to declare.

Acknowledgements

We thank Débora. Muñóz for her tecnical assitance and Hector Terán for his preliminary contribution to these studies. We are grateful to the Nikon A1R Laser Microscopy Unit of the IDIVAL Institute. This work has been supported by the Spanish MINECO and European Union FEDER under Projects ref. PI13/01074, PI16/000496, MAT2015-69508-P, the NanoBioApp Network Ref. MINECO-17-MAT2016-81955-REDT, IDIVAL Projects ref. INNVAL15/16, INNVAL 17/11, PREVAL 16/03, and the Raman4clinics BMBS COST Action BM1401.

References

1 S. Marchesan, K. Kostarelos, A. Bianco and M. Prato, *Mater. Today*, 2015, **18**, 12–19.

2 L. Lacerda, J. Russier, G. Pastorin, M. A. Herrero, E. Venturelli, H. Dumortier, K. T. Al-Jamal, M. Prato, K. Kostarelos and A. Bianco, *Biomaterials*, 2012, **33**, 3334–3343.

3 X. Deng, G. Jia, H. Wang, H. Sun, X. Wang, S. Yang, T. Wang and Y. Liu, *Carbon N. Y.*, 2007, **45**, 1419–1424.

4 J. T. W. Wang, C. Fabbro, E. Venturelli, C. Menard-Moyon, O. Chaloin, T. Da Ros, L. Methven, A. Nunes, J. K. Sosabowski, S. J. Mather, M. K. Robinson, J. Amadou, M. Prato, A. Bianco, K. Kostarelos and K. T. Al-Jamal, *Biomaterials*, 2014, **35**, 9517–28.

5 D. Pantarotto, J.-P. Briand, M. Prato and A. Bianco, *Chem. Commun. (Camb).*, 2004, 16–17.

6 P. C. B. De Faria, L. I. Dos Santos, J. P. Coelho, H. B. Ribeiro, M. A. Pimenta, L. O. Ladeira, D. A. Gomes, C. A. Furtado and R. T. Gazzinelli, *Nano Lett.*, 2014, **14**, 5458–5470.

7 A. Masotti, M. R. Miller, A. Celluzzi, L. Rose, F. Micciulla, P. W. F. Hadoke, S. Bellucci and A. Caporali, *Nanomedicine Nanotechnology, Biol. Med.*, 2016, **12**, 1511–1522.

8 N. Iturrioz-Rodríguez, E. González-Domínguez, E. González-Lavado, L. Marín-Caba, B. Vaz, M.- Pérez-Lorenzo, M. A. Correa-Duarte, M. L. Fanarraga, *Angew. Chemie Int. Ed.*, 2017, **56**, 13736–13740.

9 V. Castagnola, J. Cookman, J. M. de Araújo, E. Polo, Q. Cai, C. P. Silveira, Ž. Krpetić, Y. Yan, L. Boselli and K. A. Dawson, *Nanoscale Horiz.*, 2017, **2**, 187–198.

10 F. Pampaloni and E. L. Florin, *Trends Biotechnol.*, 2008, **26**, 302–310.

11 L. Rodríguez-Fernández, R. Valiente, J. González, J. C. Villegas and M. L. Fanarraga, *ACS Nano*, 2012, **6**, 6614–6625.

12 M. A. Jordan and L. Wilson, *Curr. Opin. Cell Biol.*, 1998, **10**, 123–130.

13 D. J. Odde, L. Ma, A. H. Briggs, A. DeMarco and M. W. Kirschner, *J. Cell Sci.*, 1999, **112**, 3283–3288.

14 P. J. de Pablo, I. A. T. Schaap, F. C. MacKintosh and C. F. Schmidt, *Phys. Rev. Lett.*, 2003, **91**, 98101.

15 C. Z. Dinu, S. S. Bale, G. Zhu and J. S. Dordick, *Small*, 2009, **5**, 310–315.

16 L. García-Hevia, F. Fernández, C. Grávalos, A. García, J. C. Villegas and M. L. Fanarraga, *Nanomedicine*, 2014, **9**, 1581–1588.

17 C. Dong, R. Eldawud, L. M. Sargent, M. L. Kashon, D. Lowry, Y. Rojanasakul and C. Zoica Dinu, *J. Mater. Chem. B*, 2015, **3**, 3983–3992.

18 L. Garcia-Hevia, R. Valiente, J. L. Fernandez-Luna, E. Flahaut, L. Rodriguez-Fernandez, J. C. Villegas, J. Gonzalez and M. L. Fanarraga, *Adv. Healthc. Mater.*, 2015, **4**, 1640–1644.

19 L. García-Hevia, R. Valiente, J. González, J. Fernández-Luna, J. C. Villegas and M. L. Fanarraga, *Curr. Pharm. Des.*, 2015, **21**, 1920–1929.

20 L. García-Hevia, J. C. Villegas, F. Fernández, Í. Casafont, J. González, R. Valiente and M. L. Fanarraga, *Adv. Healthc. Mater.*, 2016, **5**, 1–21.

21 C. Fabbro, H. Ali-Boucetta, T. Da Ros, K. Kostarelos, A. Bianco and M. Prato, *Chem. Commun.*, 2012, **48**, 3911.

22 S. Y. Madani, A. Mandel and A. M. Seifalian, *Nano Rev.*, 2014, **4**, 1–16.

23 S. Rittinghausen, A. Hackbarth, O. Creutzenberg, H. Ernst, U. Heinrich, A. Leonhardt and D. Schaudien, *Part. Fibre Toxicol.*, 2014, **11**, 59.

24 K. Kostarelos, *Nat. Biotechnol.*, 2008, **26**, 774–6.

25 J. K. Lee, B. C. Sayers, K.-S. Chun, H.-C. Lao, J. K. Shipley-Phillips, J. C. Bonner and R. Langenbach, *Part. Fibre Toxicol.*, 2012, **9**, 14.

26 R. F. Hamilton, Z. Wu, S. Mitra, P. K. Shaw and A. Holian, *Part. Fibre Toxicol.*, 2013, **10**, 57.

27 V. E. Kagan, N. V Konduru, W. Feng, B. L. Allen, J. Conroy, Y. Volkov, I. I. Vlasova, N. a Belikova, N. Yanamala, A. Kapralov, Y. Y. Tyurina, J. Shi, E. R. Kisin, A. R. Murray, J. Franks, D. Stolz, P. Gou, J. Klein-Seetharaman, B. Fadeel, A. Star and A. a Shvedova, *Nat. Nanotechnol.*, 2010, **5**, 354–359.

28 W. Seo, A. A. Kapralov, G. V Shurin, M. R. Shurin, V. E. Kagan and A. Star, *Nanoscale*, 2015, **7**, 8689–8694.

29 A. A. Shvedova, A. A. Kapralov, W. H. Feng, E. R. Kisin, A. R.

Murray, R. R. Mercer, C. M. St. Croix, M. a. Lang, S. C. Watkins, N. V. Konduru, B. L. Allen, J. Conroy, G. P. Kotchey, B. M. Mohamed, A. D. Meade, Y. Volkov, A. Star, B. Fadeel and V. E. Kagan, *PLoS One*, 2012, **7**, e30923.

30 C. Farrera, K. Bhattacharya, B. Lazzaretto, F. T. Andón, K. Hultenby, G. P. Kotchey, A. Star and B. Fadeel, *Nanoscale*, 2014, **6**, 6974–83.

31 F. T. Andón, A. A. Kapralov, N. Yanamala, W. Feng, A. Baygan, B. J. Chambers, K. Hultenby, F. Ye, M. S. Toprak, B. D. Brandner, A. Fornara, J. Klein-Seetharaman, G. P. Kotchey, A. Star, A. A. Shvedova, B. Fadeel and V. E. Kagan, *Small*, 2013, **9**, 2721–9, 2720.

32 D. Elgrabli, W. Dachraoui, C. Menard-Moyon, X. J. J. Liu, D. Begin, S. Begin-Colin, A. Bianco, F. Gazeau and D. Alloyeau, *ACS Nano*, 2015, **9**, 10113–10124.

33 M. Meneghetti, A. Bianco, A. Nunes, C. Bussy, L. Gherardini, M. Meneghetti, M. A. Herrero, A. Bianco, M. Prato, T. Pizzorusso, K. T. Al-Jamal, K. Kostarelos, A. A. Herrero, A. Bianco, M. Prato, T. Pizzorusso, K. T. Al-Jamal, K. Kostarelos, L. Gherardini, M. Meneghetti, M. A. Herrero, A. Bianco, M. Prato, T. Pizzorusso, K. T. Al-Jamal and K. Kostarelos, *Nanomedicine*, 2012, **7**, 1485–1494.

34 C. Bussy, C. Hadad, M. Prato, A. Bianco and K. Kostarelos, *Nanoscale*, 2016, 590–601.

35 A. E. Goode, D. A. Gonzalez Carter, M. Motskin, I. S. Pienaar, S. Chen, S. Hu, P. Ruenraroengsak, M. P. Ryan, M. S. P. Shaffer, D. T. Dexter and A. E. Porter, *Biomaterials*, 2015, **70**, 57–70.

36 J. Russier, L. Oudjedi, M. Piponnier, C. Bussy, M. Prato, K. Kostarelos, B. Lounis, A. Bianco and L. Cognet, *Nanoscale*, 2017, **9**, 4642–4645.

37 I. I. Vlasova, T. V. Vakhrusheva, A. V. Sokolov, V. A. Kostevich, A. A. Gusev, S. A. Gusev, V. I. Melnikova and A. S. Lobach, *Toxicol. Appl. Pharmacol.*, 2012, **264**, 131–142.

38 N. Lu, J. Li, R. Tian and Y. Y. Peng, *Chem. Res. Toxicol.*, 2014, **27**, 1070–1077.

39 J. C. Villegas, L. Álvarez-Montes, L. Rodríguez-Fernández, J. González, R. Valiente and M. L. Fanarraga, *Adv. Healthc. Mater.*, 2014, **3**, 424–432.

40 O. Vittorio, V. Raffa and A. Cuschieri, *Nanomedicine Nanotechnology, Biol. Med.*, 2009, **5**, 424–431.

41 J. Hou, B. Wan, Y. Yang, X.-M. Ren, L.-H. Guo and J.-F. Liu, *Int. J. Mol. Sci.*, 2016, **17**, 409.

42 V. E. Kagan, A. A. Kapralov, C. M. St Croix, S. C. Watkins, E. R. Kisin, G. P. Kotchey, K. Balasubramanian, I. I. Vlasova, J. Yu, X. Kang Kim, X. Wanji Seo, R. K. Mallampalli, A. Star and A. A. Shvedova, *ACS Nano*, 2014, **8**, 5610–5621.

43 N. Saito, H. Haniu, Y. Usui, K. Aoki, K. Hara, S. Takanashi, M. Shimizu, N. Narita, M. Okamoto, S. Kobayashi, H. Nomura, H. Kato, N. Nishimura, S. Taruta and M. Endo, *Chem. Rev.*, 2014, **114**, 6040–6079.

44 H. Nagai, Y. Okazaki, S. Chew, N. Misawa, Y. Yamashita, S. Akatsuka, T. Ishihara, K. Yamashita, Y. Yoshikawa, H. Yasui, L. Jiang, H. Ohara, T. Takahashi, G. Ichihara, K. Kostarelos, Y. Miyata, H. Shinohara and S. Toyokuni, *Proc. Natl. Acad. Sci.*, 2011, **108**, 1330–1338.

45 A. R. Sureshbabu, R. Kurapati, J. Russier, C. Ménard-Moyon, I. Bartolini, M. Meneghetti, K. Kostarelos and A. Bianco, *Biomaterials*, 2015, **72**, 20–28.

46 A. Bianco, K. Kostarelos and M. Prato, *Chem. Commun. (Camb).*, 2011, **47**, 10182–10188. View Article Online DOI: 10.1039/C8NR03036G

47 T. M. Sager, M. W. Wolfarth, M. Andrew, A. Hubbs, S. Friend, T. Chen, D. W. Porter, N. Wu, F. Yang, R. F. Hamilton and A. Holian, *Nanotoxicology*, 2014, **8**, 317–27.

48 Y. Zhao, B. L. Allen and A. Star, *J. Phys. Chem. A*, 2011, **115**, 536–9544.

49 X. Liu, R. H. Hurt and A. B. Kane, *Carbon N. Y.*, 2010, **48**, 1961–1969.

50 J. Russier, C. Ménard-Moyon, E. Venturelli, E. Gravel, G. Marcolongo, M. Meneghetti, E. Doris and A. Bianco, *Nanoscale*, 2011, **3**, 893–896.

51 X. Zhuang, X. Xiang, W. Grizzle, D. Sun, S. Zhang, R. C. Axtell, S. Ju, J. Mu, L. Zhang, L. Steinman, D. Miller and H.-G. Zhang, *Mol. Ther.*, 2011, **19**, 1769–79.

52 J. Zhang, H. L. Zou, Q. Qing, Y. L. Yang, Q. W. Li, Z. F. Liu, X. Y. Guo and Z. L. Du, *J. Phys. Chem. B*, 2003, **107**, 3712–3718.

53 U. J. Kim, C. A. Furtado, X. Liu, G. Chen and Peter C. Eklund, *J. Am. Chem. Soc.*, 2005, **127**, 15437–15445.

54 R. M. Silverstein, G. C. Bassler and T.C. Morrill, in *Spectrometric Identification of Organic Compounds, 4th ed. New York, John Willey and Sons*, 1981.

55 E. F. Antunes, a. O. Lobo, E. J. Corat, V. J. Trava-Airoldi, a. a. Martin and C. Veríssimo, *Carbon N. Y.*, 2006, **44**, 2202–2211.

56 C. Dong, A. S. Campell, R. Eldawud, G. Perhinschi, Y. Rojanasakul and C. Z. Dinu, *Appl. Surf. Sci.*, 2013, **264**, 261–268.

57 A. M. Rao, P. C. Eklund, S. Bandow, A. Thess and R. E. Smalley, *Nature*, 1997, **388**, 257–259.

58 S. Gupta, M. Hughes, A. H. Windle and J. Robertson, *J. Appl. Phys.*, 2004, **95**, 2038–2048.

59 C. Bussy, A. Bianco, M. Prato and K. Kostarelos, *Nanoscale Horizons*, 2017, **2**, 284–296.

60 G. Poste, J. Doll, I. R. Hart and I. J. Fidler, *Cancer Res.*, 1980, **40**, 1636–1644.

61 L. García-Hevia, F. Fernández, I. Casafont, J. C. Villegas and M. L. Fanarraga, *Biomed. Phys. Eng. Express*, 2016, **2**, 35009.

62 E. Flahaut, C. Laurent and A. Peigney, *Carbon N. Y.*, 2005, **43**, 375–383.

63 M. S. Dresselhaus, G. Dresselhaus, R. Saito and a. Jorio, *Phys. Rep.*, 2005, **409**, 47–99.

64 M. S. Dresselhaus and P. C. Eklund, *Adv. Phys.*, 2000, **49**, 705–814.

View Article Online
DOI: 10.1039/C8NR03036G

TOC graphic

Mild oxidation treatments improve *in vitro* and *in vivo* macrophage biodegradation of carbon nanotubes that trigger remarkable anti-tumoral effects in malignant melanoma solid tumors produced mice.